RSC Advances

ROYAL SOCIETY OF CHEMISTRY

www.rsc.org/advances

Electric, Magnetic, Piezoelectric and Magnetoelectric Studies of phase pure ($BiFeO_3$-$NaNbO_3$)-(P(VDF-TrFE)) Nanocomposite films prepared by spin coating

Rehana P Ummer[a], Raneesh. B[d], Camille Thevenot[e,f], Didier Rouxel[e,f], Sabu Thomas[b,c], Nandakumar Kalarikkal[a,c],

[a]*School of Pure and Applied Physics,* [b]*School of Chemical Sciences,* [c]*International and Inter University Centre for Nanoscience and Nanotechnology*

Mahatma Gandhi University, Kottayam, Kerala-686560, India

[d]*Department of Physics, Catholicate College, Pathanamthitta, Kerala-689645, India*

[e]*Université de Lorraine, Institut Jean Lamour, Vandoeuvre-lès-Nancy, F-54506, France*

[f]*CNRS, IJL UMR7198, Vandoeuvre-lès-Nancy, F-54506, France*

Abstract

($BiFeO_3$-$NaNbO_3$)-(P(VDF-TrFE)) co-polymer thin films were fabricated by spin coating technique and their electric, magnetic, electromechanical and magnetoelectric properties were investigated. In order to get the crystallization 'β' phase, the films have been annealed at 138^o C. The structural analysis of the films have been carried out using XRD, SEM, TEM, AFM, Confocal Raman spectroscopy and FTIR spectroscopy which confirm the presence of $BiFeO_3$ and $NaNbO_3$ phases along with P(VDF-TrFE) crystalline phase. The magnetoelectric coupling measurements at room temperature confirm the multiferroic nature of the composite film with significant magnetoelectric coupling between $BiFeO_3$, $NaNbO_3$ and P(VDF-TrFE). The ME measurement give a maximum coupling coefficient of 2.4 V/cmOe for the ceramic-polymer composite film which is two times higher than that of the ceramic alone. The higher piezoelectricity of the P(VDF-TrFE) (d_{33} > 20 pC/N) is expected to contribute to the enhancement in electric and magnetic properties of the composite. The hysteresis loop observed at room temperature confirms the ferromagnetic property of the composite. The ultrahigh dielectric constant for 10 vol % of the ceramic in the polymer matrix with low loss value (≈1) is a remarkable improvement. The resultant high dielectric permittivity, magneto electric coupling and ferromagnetic property at room temperature of these innovative nanocomposites make them particularly attractive for technological applications as storage energy materials.

Keywords: Multiferroic, Magnetoelectric coupling coefficient, Piezoelectric coefficient

E-mail: nkkalarikkal@mgu.ac.in, Tel: +919447671962, Fax: +91481-2731669, Mail address: School of Pure and Applied Physics, Mahatma Gandhi University, Kottayam, Kerala 686 560, India

1. Introduction

Multiferroic thin films are technologically important in spintronic devices due to low power consumption.[1-11] However, the origin of ferroelectricity in single-phase multiferroics is largely unrelated to the magnetic order, and the magnetoelectric (ME) coupling observed at room temperature in these materials is still too weak to be useful for device design.[12] To overcome the limitations of single-phase multiferroics, composite and multilayer multiferroics consisting of coupled magnetic and ferroelectric phases are promising to show higher magnetization values. Now research domains focuses on artificial engineered piezoelectric/magnetoelectric bilayers in which magnetization is controlled by an electric field.[13-16] Room temperature multiferroicity has been intensively investigated in laminates and bilayer thin films.[17-22] The origin of magnetoelectric (ME) coupling in bilayer and epitaxial films arises due to magnetostriction and piezoelectricity.[23-27] Indeed in these kind of bilayers a significant magnetoelectrtic coupling is obtained only in the presence of non-negligible in-plane stresses in the magnetic media.[28-36]

Such ME composites fabricated by combining piezoelectric and magnetostrictive materials have drawn significant recent interest due to their multifunctionality, in which the coupling interaction between the piezoelectric and magnetostrictive phases produce a large ME response. [37]
The ME coefficients obtained in these ceramic particulate or laminated composites are typically three orders of magnitude higher than in single phase materials.[38-40] On the other hand ceramic composites may become fragile and are limited by deleterious reactions at the interface regions leading to low electrical resistivity and high dielectric losses (>0.1), hindering in this way the incorporation into devices of these materials.[41] A promising and less explored approach to obtain a good ME coupling is the development of particulate composites within a polymer matrix where the polymer matrix is the piezoelectric phase. Polyvinylidene fluoride (PVDF) and it's copolymers have the best electroactive performance in the small class of polymers displaying piezo, pyro and ferroelectricity. The PVDF polymer can be characterized as a light, compliant material which exhibits considerable dielectric strength, high sensitivity to mechanical loads and

stable piezoelectric properties in diverse chemical environments.[42,43] Due to these qualities, PVDF and P(VDF-TrFE) have been increasingly used in a variety of applications, particularly in such devices as sensors and transducers.[44-49] These properties are originated from the strong molecular dipoles within the polymer chains. A large magnetoelectric coupling coefficient of 12 V/cmOe was observed in polyvinylidene fluoride-hexafluoropropene, (PVDF-HFP) co-polymers.[50]

Nanocomposite thin films composed of ferrimagnetic cobalt ferrite nanocrystals and a ferroelectric/piezoelectric polymer PVDF-HFP prepared by spin coating also shows very good magneto electric coupling at room temperature.[51] There are various reports showing sudden increase of magnetoelectric coupling coefficient in layered composites which arises due to piezoelectricity.[52-56] Polyvinylidene fluoride (PVDF) and poly vinylidene fluoridene-trifluorethylene (P(VDF-TrFE)) have received special attention as the incorporation of this ferroelectric, piezoelectric polymer enhance the dielectric property of the composite.[57-59]

P(VDF-TrFE) matrix nanocomposites loaded with nanoparticles of metal oxides and others have been specially studied recently.[60-63] Even if most of the pure polymers show low dielectric constant, PVDF and its co-polymer P(VDF-TrFE) have high dielectric constant which leads to good magnetoelectric coupling property.[46,47, 64,65] It makes them more attractive in electronic and electrical industry due to their inherent advantages in flexibility, easy processing, low coast and high breakdown strength. Therefore a great deal of effort has gone into the development of ceramic–polymer composites, which are formed by suspending ceramic powders into a polymer matrix. The created composites combine the advantages of ceramics and polymers, and represent a novel type of material that is flexible and easy to process and is of relatively high dielectric constant and high breakdown strength.

2. Experimental procedure

The ceramic nanopowder and polymer solution is prepared separately and then both mixed together in different nanoparticle concentrations. The film samples were prepared in different steps. The preparation technique is detailed below.

2.1 Preparation of $BiFeO_3$-$NaNbO_3$ composite powder

Stoichiometric powders of (0.9)$BiFeO_3$-(0.1)$NaNbO_3$ ceramics were synthesized from analytical grade (Aldrich) $BiNO_3$, $FeNO_3$, $NaNO_3$, $C_4H_4NNbO_9$ using pechini method.[66] The precursors

were dissolved in double distilled water and citric acid was added to the solution with nitrates to citric acid molar ratio 1:1 and heated at 80-90^{o} C for the gelation process. The obtained gel was heated at 500^{o} C for 1 hour and final sintering was done at 850^{o} C.

2.2 Thin film preparation

After cleaning process, the glass substrates are metalized by e-beam evaporation with 10 nm of Chromium (sticking layer) and 70 nm of Gold. Then the copolymer P(VDF-TrFE) is dissolved in MEK (Methyl Ethyl Ketone) at a concentration of 14 wt %. The (0.9)$BiFeO_3$-(0.1)$NaNbO_3$ ceramic powder is dissolved in the polymer solution in the following concentrations.

Table 1 : Details of the film samples

Sl. No.	Concentration (wt%) of ceramic particle	Volume of copolymer solution (mL)	Mass of copolymer (mg)	Mass of nanoparticles (mg)
1	0 %	4	468	0
2	5 % $BiFeO_3$	4	468	24.6
3	5 % $BiFeO_3$-$NaNbO_3$	4	468	24.6
4	10% $BiFeO_3$-$NaNbO_3$	4	468	52

All the solutions were treated by ultrasonication (Transducer Digital Sonifier Model 450, Brandson Ultrasonics Corporation) with action time 1 min 30 s, a power of 120 W (30 % of the maximum power) and a pulse on/off 0.1/0.1 (s/s). The container bottles are put in ice throughout the process. Directly after the ultrasonication process the solutions are spin coated in two steps. In the first step rotation speed of 500 rpm, acceleration 125 rpm/s and time 10 s are used. In the second step rotation speed of 1500 rpm, acceleration 125 rpm/s and time 40 s are used. Then the samples put directly at 138^{o} C for 1 hour to get the crystallization phase and cooled down to room temperature. The corona process parameters are 12 kV set-up voltage and 6 min duration. The upper metallization is done for deposition of a 10 mm Cr/Au disk in the same apparatus used for the lower electrode but under a polymide (Kapton) mask. A typical configuration of the sample is shown in Fig. 1.

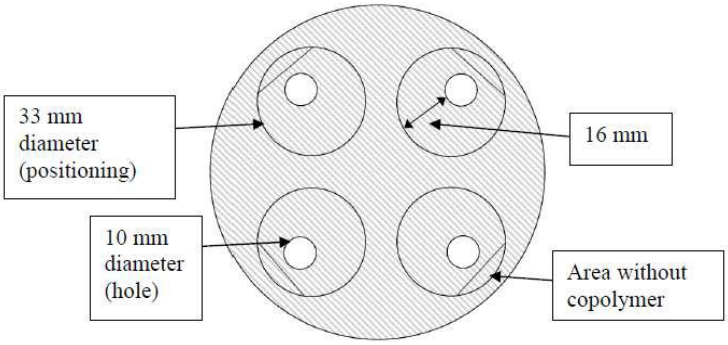

Fig. 1 The typical configuration of the prepared thin film sample

The crystal structures of the samples were examined by Phillips X'Pert Pro XRD with Cu-Kα radiation (1.54056Å). Step scanned powder XRD data was collected in the 2θ range 10^o-80^o at room temperature. Detailed structural analysis was performed using SEM (JEOL JSM 6390), Transmission Electron Microscope (JEOL JEM 2100) and FTIR spectroscopy. The piezoelectric property was determined by PFM using SS01 Piezo-d meter, (Sensor Technologie Limited). A conventional ME measurement has been carried out using the lock in amplifier method[67] and room temperature dielectric studies were performed using an Agilent 4980 precision LCR meter. The magnetization measurements were performed using Vibrating Sample Magnetometer.

3. Results and discussion

3.1 Structural analysis

Fig. 2 (a) shows the crystal structure of different phases of PVDF.[93] Among the various crystalline phases of PVDF, α and β phases are predominant. Our interest was on electroactive β phase which can alter the electric behavior. The parallel alignment of dipoles in the β phase create a net surface charge while the net surface charge is zero in α phase as the dipoles cancel out each other due to the random orientation. The phase structure of the film was examined using X-ray diffraction techniques. Fig. 2(b) shows X-ray diffractograms at room temperature of the P(VDF-TrFE)-$BiFeO_3$-$NaNbO_3$ composite films. For the as-cast film a sharp diffraction peak of (200) and (110) planes at 19.9^o and 38^o (marked by 'P') attributed to ferroelectric ß phase of P(VDF-TrFE) and are consistent with previously reported results for P(VDF-TrFE) with other molar compositions.[13,36,48-51]

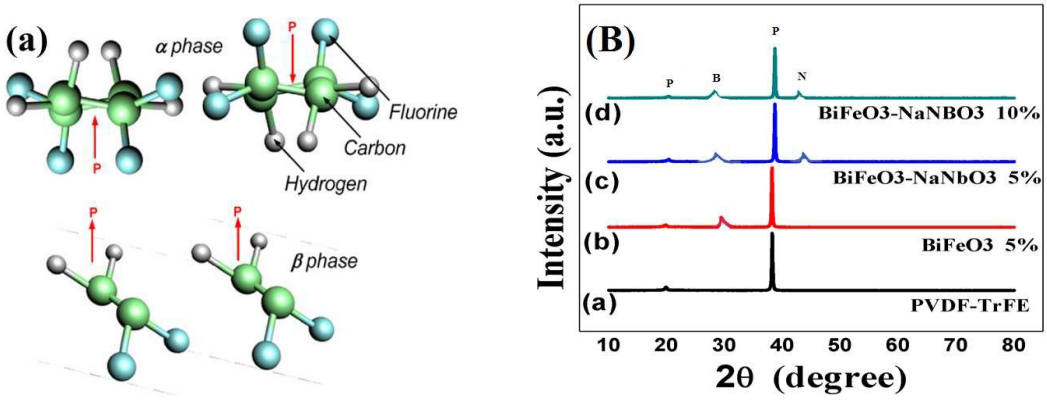

Fig. 2 (a) Crystal structure of PVDF different phases, (b) X-ray diffractogram of composite film samples for various nanoparticle concentrations in the polymer matrix.

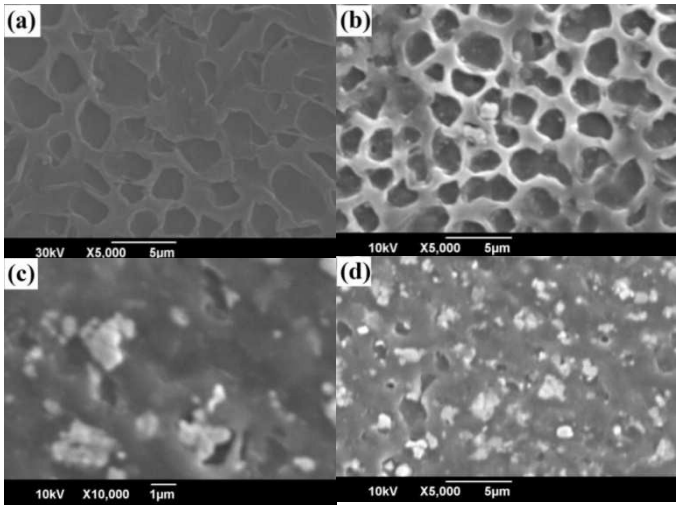

Fig. 3 SEM images of $BiFeO_3$-$NaNbO_3$–P(VDF–TrFE) composite film samples for, (a) P(VDF-TrFE) alone, (b) 5% $BiFeO_3$ in the P(VDF-TrFE) matrix, (c) 5% $BiFeO_3$-$NaNbO_3$ in the P(VDF-TrFE) matrix, (d) 10% $BiFeO_3$-$NaNbO_3$ in the P(VDF-TrFE) matrix.

The other peaks marked by 'B' and 'N' correspond to $BiFeO_3$ and $NaNbO_3$ phases respectively. The average crystalline size of nanoparticle found from Scherrer equation varies between 100 nm to 150 nm. Fig. 3 shows the SEM images of the as-sintered surfaces of the film. From the SEM images we can observe the nanoparticle aggregates on the polymer matrices. Fig. 4 (a) and 4(b) shows the TEM images of the film samples.

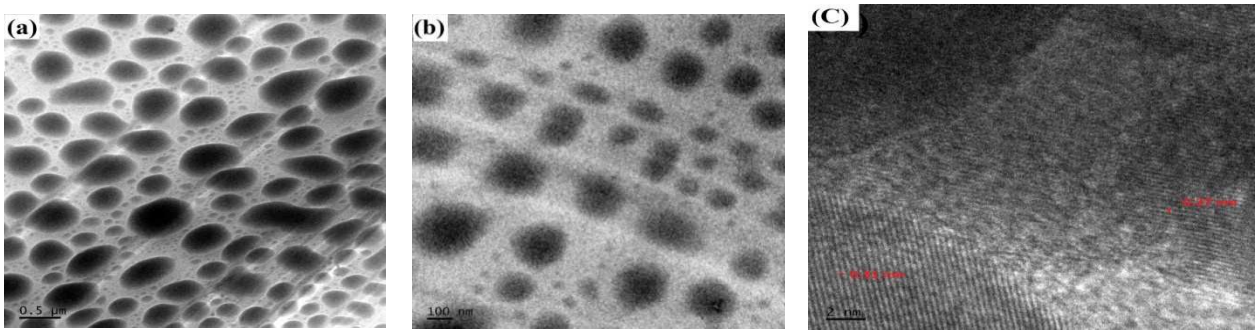

Fig. 4 TEM images of $BiFeO_3$-$NaNbO_3$- P(VDF-TrFE) composite film samples for (a) 5 % $BiFeO_3$ in the polymer matrix (b) 5% $BiFeO_3$-$NaNbO_3$ in the polymer matrix (c) HRTEM image of 5 % $BiFeO_3$ - $NaNbO_3$ in the polymer matrix.

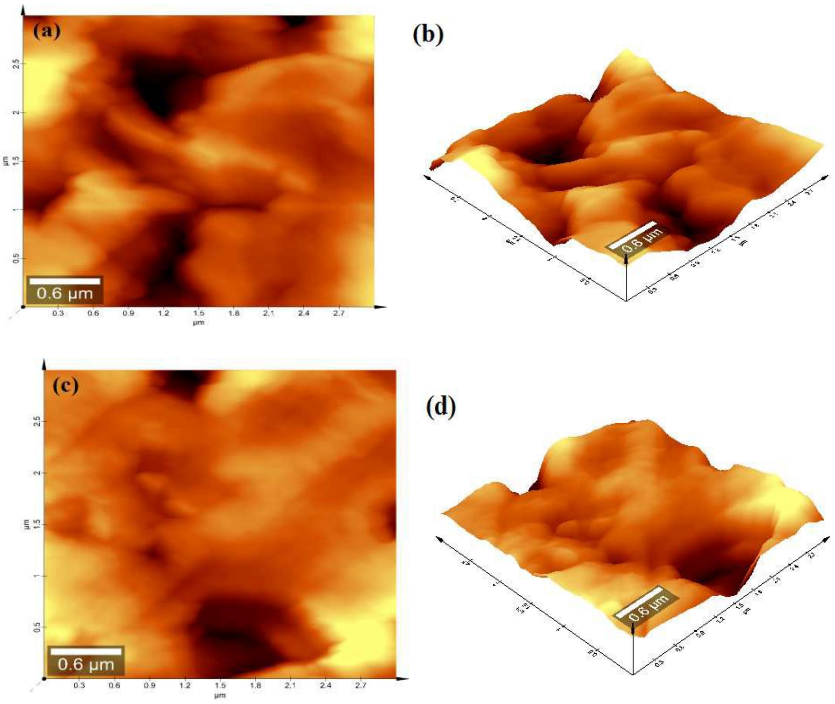

Fig. 5 (a) 2D AFM image of 5% $BiFeO_3$-$NaNbO_3$ in the polymer matrix, (b) 3D AFM image of 5% $BiFeO_3$-$NaNbO_3$ in the polymer matrix, (c) 2D AFM image of 10% $BiFeO_3$-$NaNbO_3$ in the polymer matrix, (d) 3D AFM image of 10% $BiFeO_3$-$NaNbO_3$ in the polymer matrix

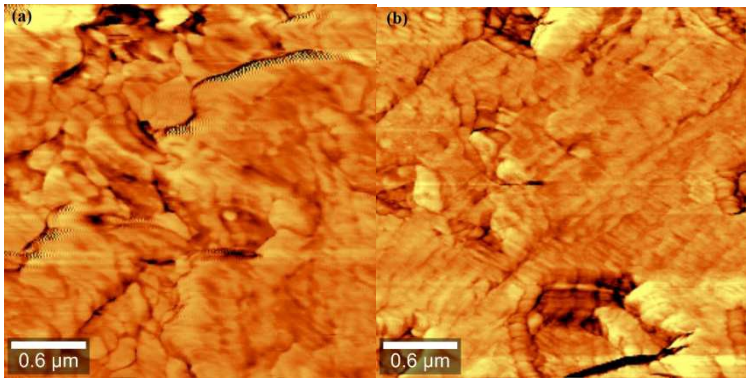

Fig. 6 The phase images of the samples (a) 5% $BiFeO_3$-$NaNbO_3$ in polymer matrix, (b) 10% $BiFeO_3$-$NaNbO_3$ in polymer matrix.

Fig 4 (c) shows HRTEM of 5% $BiFeO_3$ - $NaNbO_3$ in the polymer matrix which clearly indicates the polycrystalline nature of the film sample. The lattice spacing (d) calculated from the HRTEM image matches with JCPDS values corresponding to $BiFeO_3$ and $NaNbO_3$. The d values of 0.27 nm and 0.31 nm corresponds to (110) and (131) planes of rhombohedral $BiFeO_3$ (JCPDS 74-2016) and orthorhombic $NaNbO_3$ (JCPDS 89-8957 respectively. Fig. 5 shows the AFM images of the film samples. Here, the surface morphology was studied with AFM by taking account of the composite surface. In the 3D AFM picture, we can observe the surface roughness. Fig. 6 shows AFM phase images of samples with 5% and 10% $BiFeO_3$-$NaNbO_3$ in polymer matrix. The force exerted by the AFM tip on the surface will be different for the nano particle and the polymer surface and the phase image may represents the different particles/phases, if present. The force exerted by the AFM tip on the surface will be different for the nano particle and the polymer surface. In the present case a sharp distinction between the polymer and nanoparticles cannot be made as there is no much differences in the phase images.

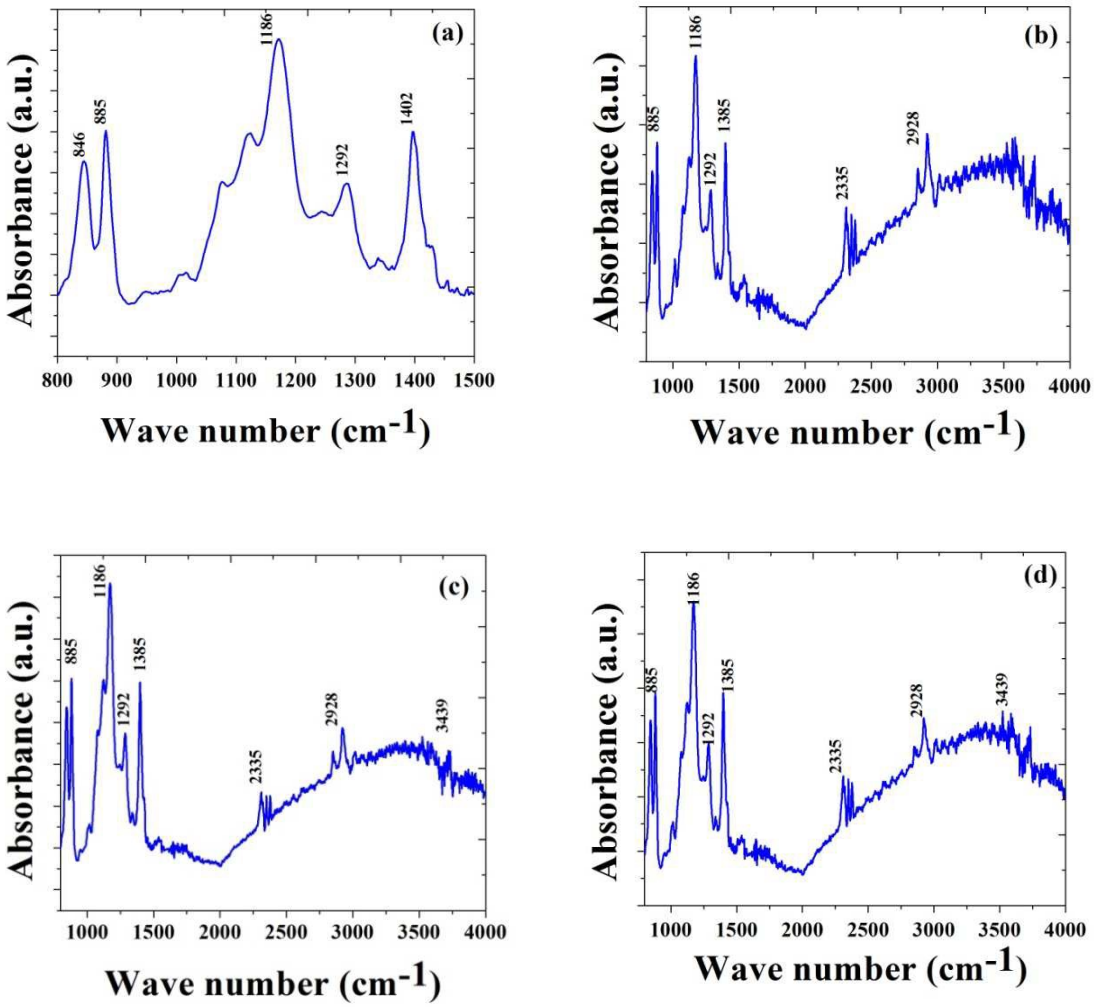

Fig. 7 FTIR spectra of ($BiFeO_3$-$NaNbO_3$)-P(VDF-TrFE) composite film samples for (a) P(VDF-TrFE) alone, (b) 5% $BiFeO_3$ in the P(VDF-TrFE) matrix, (c) 5% $BiFeO_3$-$NaNbO_3$ in the P(VDF-TrFE) matrix, (d) 10% $BiFeO_3$-$NaNbO_3$ in the P(VDF-TrFE) matrix.

Inorder to have more detailed interpretation of the structure of ceramic composite film samples, FTIR spectroscopy is used (Fig. 7). Several vibrational bands for the co-polymer have been assigned to specific confirmations by previous reports.[68-71] Characteristic absorption bands due to the electro active ß phase at 885 cm^{-1} (CH_2 rocking, CF_2 stretching and skeletal C-C stretching) have been found. The band at 1402 cm^{-1}, 1292 cm^{-1}, 1186 cm^{-1}, 885 cm^{-1}, 848 cm^{-1} are associated with crystalline phase (ß) of P(VDF–TrFE) co polymer which shows marginal increase in the absorption intensity irrespective of the nanoparticle addition in the polymer film. From the report of Kim.et al,[71] it was observed that the changes in the intensity at 1292 cm^{-1} bands is highly dependent on the amount of ferroelectric phase content and can be suitable candidate for monitoring the ferroelectric crystalline phase.[71] The bands at 3439 cm^{-1}, 2928 cm^{-}

[1], 2335 cm^{-1} and 1385 cm^{-1} are due to the ceramic nano particle. The broad absorption band in the range of 3439 cm^{-1} is assigned to O-H stretching and the 2928 cm^{-1} band is due to C-H stretching vibrations. A peak at 2335 cm^{-1} was representative of nitrile[72] and the band located at 1385 cm^{-1} indicate the existence of nitrate ions.[67, 73-74]

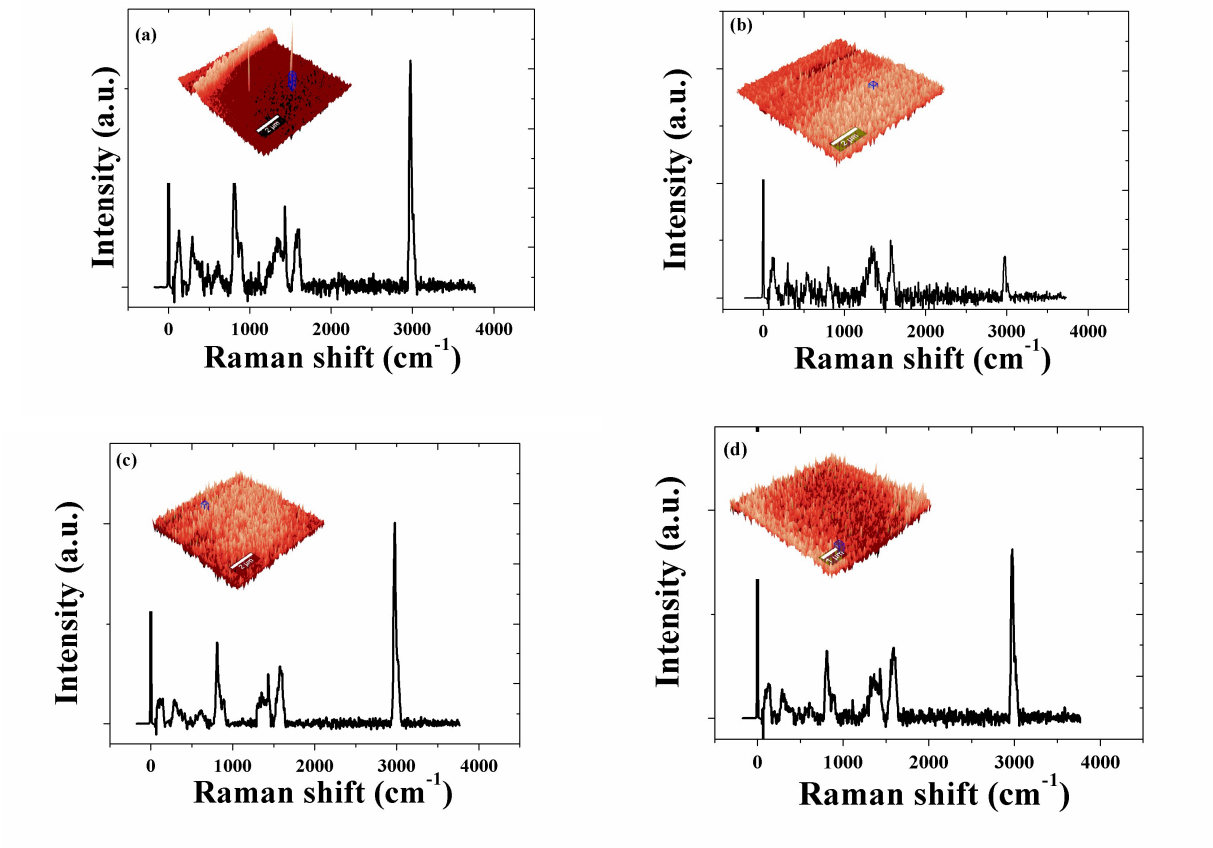

Fig. 8 Confocal raman spectra of $BiFeO_3$-$NaNbO_3$-P(VDF-TrFE) composite film samples for (a) P(VDF-TrFE) alone, (b) 5 % $BiFeO_3$ in the P(VDF-TrFE) matrix, (c) 5 % $BiFeO_3$-$NaNbO_3$ in the P(VDF-TrFE) matrix, (d) 10% $BiFeO_3$-$NaNbO_3$ in the P(VDF-TrFE) matrix.

The Raman spectra and corresponding Raman images of the samples are shown in Fig. 8. The intensity of the peak from PVDF absorbance (1430 cm^{-1}) remains unaltered in all the spectra. Raman spectra also confirm the presence of β phase crystal domains of P(VDF-TrFE) through out the films. By group theory, there are 13 active Raman modes present in BFO for rhombohedral R3c structure. In our samples characteristic modes at 132 cm^{-1}, 169 cm^{-1}, 221 cm^{-}

[1], 254 cm^{-1} are dominated by the Bi-O covalent bonds and these four characteristic modes results the origin of ferroelectric order in the composite. The other modes which lie between 300 cm^{-1} to 600 cm^{-1} are characteristic modes of $BiFeO_3$.[75] Because of local stress and a large number of point defects, several fundamental modes are not detected in the spectrum. The Raman modes in the low wavenumber region 150–300 cm^{-1} are characteristic of the bending modes of Nb–O–Nb, whereas the band at 992 cm^{-1} is due to a small concentration of the Nb=O surfaces.[76-78] The Raman band in the range of 500–700 cm^{-1} (612 cm^{-1}) and 150–300 cm^{-1} (251 cm^{-1}) are assigned to the Nb–O–Nb vibrations of the NbO_6 octahedrons present in the crystalline structure of $NaNbO_3$. Moreover, the peak at about 871 cm^{-1} is related to the Nb–O vibrations of isolated octahedras.[79]

The inset shows corresponding confocal Raman images. The conventional Raman imaging method using a narrow spectral range corresponding to a characteristic Raman band of each chemical species is adopted. The contrast and resolution of Raman images can be greatly increased by positioning a sharp silver tip near the laser focus. The simultaneously recorded topographic 3D image is presented in the inset of each spectrum. The bright field region of the Raman image represents the nanoparticles and dark region represents the P(VDF-TrFE) matrix.

3.2 Piezoelectric and magnetoelectric studies

Fig. 9 shows the topographic and PFM images of 5% $BiFeO_3$- $NaNbO_3$ and 10% $BiFeO_3$-$NaNbO_3$ in PVDF-TrFE matrix. The topographic image reveals a morphologic structure consisting of grains in the nanometer size. In the vertical PFM amplitude images shown in Fig. 9(c) and 9(d), inhomogeneously distributed regions with opposite contrast are present. White and dark regions in the PFM images correspond to domains with the polarization vector oriented towards the surface of the sample and to the bottom electrode respectively.

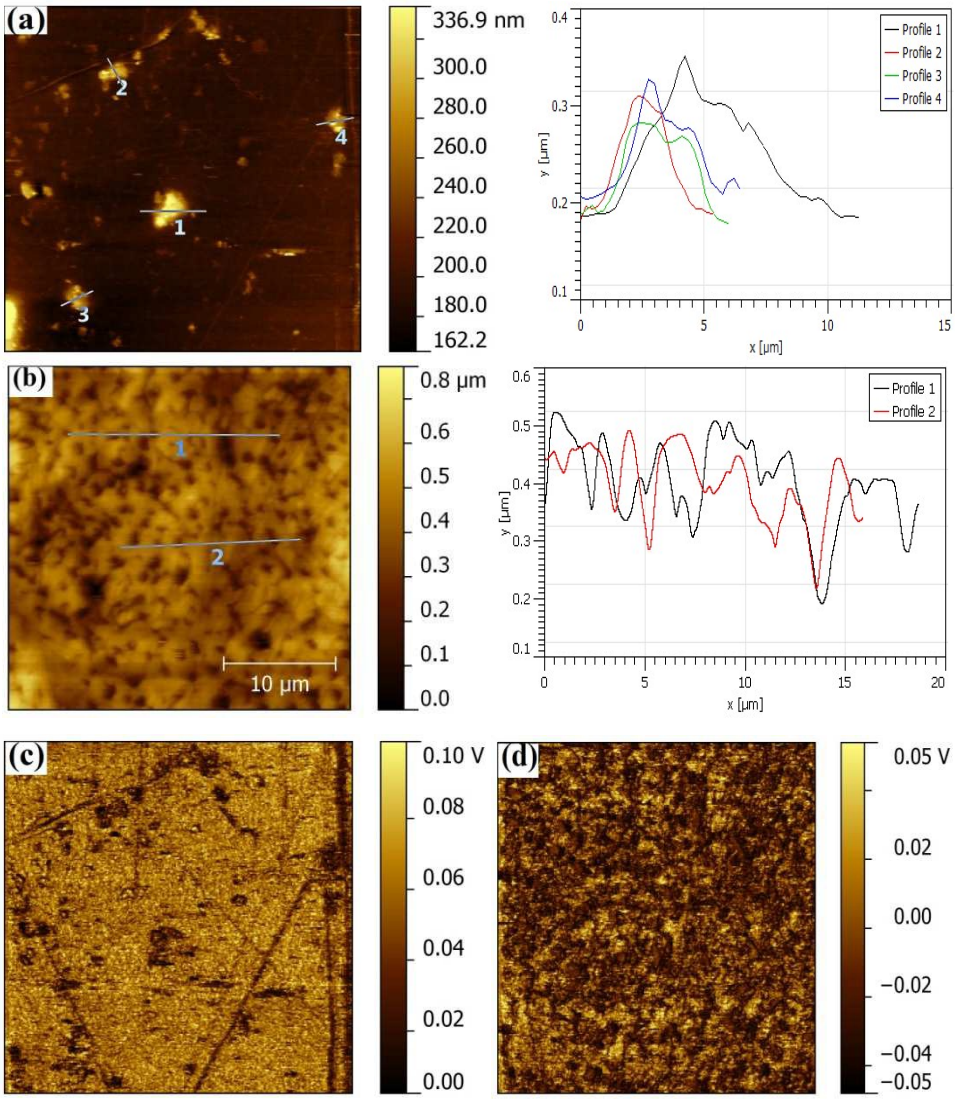

Fig. 9 (a) Surface topography of 5% $BiFeO_3$- $NaNbO_3$ in the polymer matrix (b) Surface topography of 10% $BiFeO_3$- $NaNbO_3$ in the polymer matrix (c) PFM image of 5% $BiFeO_3$- $NaNbO_3$ in the polymer matrix (d) PFM image of 10 % $BiFeO_3$- $NaNbO_3$ in the polymer matrix.

These images are reminiscent of the typical PFM contrast observed in polycrystalline ferroelectric ceramics.[80,81] Domain walls appear as narrow dark lines with a characteristically weak amplitude signal and a smallest measured width. The high value of the PFM amplitude signal suggests that the molecular chains in these crystallites are aligned parallel to the substrate. The d_{33} values were determined from the PFM images and it is found to be 34 pC/N and 38 pC/N for 5 % $BiFeO_3$- $NaNbO_3$ in P(VDF-TrFE) and 10 % $BiFeO_3$- $NaNbO_3$ in P(VDF-TrFE) respectively. This is the most important evidence that the present material is good piezoelectric.

It can be seen that the vertical piezoelectric coefficient d_{33} increases by increasing the % vol of nanoparticle in the polymer.

Table 2: The d_{33} values determined by Berlincourt method

Sl. No.	Concentration (wt%) of ceramic particle	d_{33} values (pC/N)
1	0 %	$19^{\pm 2}$
2	5 % $BiFeO_3$	$23^{\pm 2}$
3	5 % $BiFeO_3NaNbO_3$	$22^{\pm 2}$
4	10% $BiFeO_3NaNbO_3$	$21^{\pm 2}$

The piezoelectric coefficient d_{33} is also measured using the direct method often called Berlincourt method (SS01 Piezo-d meter, Sensor Technologie Limited)[82] by applying a force of 2N and the values are tabulated in Table 2. There is a slight difference in the d33 values measured by PFM technique and Berlincourt method. However, from the two techniques employed it could be clarified that the material is piezoelectric in nature. The difference in the measured values could be attributed to teh fact that in the PFM technique, the measurements have been done on the entire film sample by keeping the entire film on the sample holder and the images were taken from different regions. But in Berlincourt method, only a small portion of the sample has been peeled out and the measurements were carried out in this portion.

In layered multiferroics, the in plane stresses arouse multiferroism.[28-36] Among the various possibilities, interfacial strain coupling between the ferroelectric and magnetic phases via the piezoelectric effect is the most investigated route for the enhancement of multiferroic property in layered structures. Hence the piezoelectric property and magnetoelectric property are very much related. The piezoelectric charge coefficient d_{33} is one of the fundamental parameters defining the piezoelectric activity of a material, basically the higher the d_{33} value the more active the material is. The d_{33} coefficient is defined as the charge produced for an applied stress or the strain for an applied voltage and these are theoretically equivalent.[83]

The coexistence of electric and magnetic phases in the samples which brings about the magnetoelectric (ME) coupling was measured using a Lock-in amplifier. The A.C. magnetic field dependence of ME voltage at room temperature is shown in Fig. 10. The magnetoelectric

response for three different fixed DC field is measured. For every composition, it shows linear dependence on the applied field. The value of magnetoelectric coupling coefficient (α) is determined from the slope of the ME curve. The values of magnetoelectric coupling coefficient (α) are tabulated in Table 3. ME response of ceramic-polymer thin film shows very good result compared to the $BiFeO_3$-$NaNbO_3$ ceramic nano powder which we found in our previous experiments.[40] Here we can say that the piezoelectric polymer P(VDF-TrFE) enhances the ME response of the film samples.[36,84]

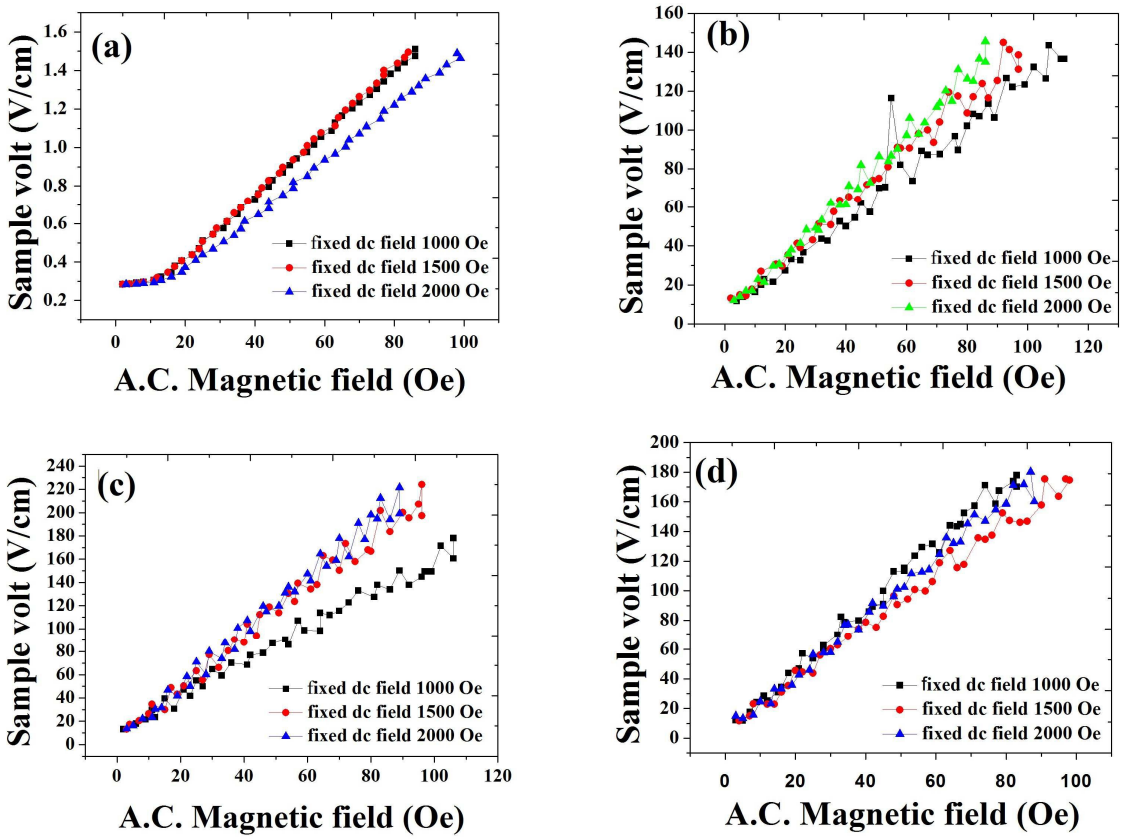

Fig. 10 ME voltage as a function of AC magnetic field at different fixed DC field for $BiFeO_3$-$NaNbO_3$ – P(VDF-TrFE) composite film samples for (a) P(VDF-TrFE) alone, (b) 5% $BiFeO_3$ in the P(VDF-TrFE) matrix, (c) 5% $BiFeO_3$-$NaNbO_3$ in the P(VDF-TrFE) matrix, (d) 10% $BiFeO_3$-$NaNbO_3$ in the P(VDF-TrFE) matrix.

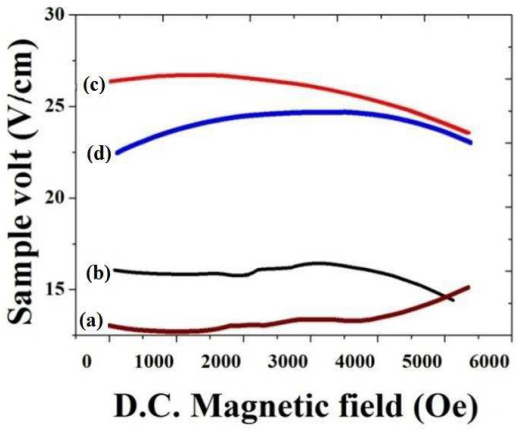

Fig. 11 ME voltage as a function of DC magnetic field for $BiFeO_3$-$NaNbO_3$-P(VDF-TrFE) composite film samples for (a) P(VDF-TrFE) alone, (b) 5 % $BiFeO_3$ in the P(VDF-TrFE) matrix, (c) 5% $BiFeO_3$-$NaNbO_3$ in the P(VDF-TrFE) matrix, (d) 10% $BiFeO_3$-$NaNbO_3$ in the P(VDF-TrFE) matrix.

Table 3 : Calculated values of magnetoelectric coupling coefficient (α)

Sl. No.	Sample Name	ME coefficient (α) (V/cmOe)	
		For fix dc 1000Oe	For fix dc 2000Oe
1	P(VDF-TrFE)	0.01	0.02
2	5% $BiFeO_3$	1.26	1.88
3	5% $BiFeO_3$-$NaNbO_3$	1.48	2.42
4	10%$BiFeO_3$-$NaNbO_3$	1.99	2.42

For increasing vol % of ceramic nanoparticles, the ME response is found to be increasing in the composite. Increase in the ME voltage according to the percentage increase of nanoparticles is explained by the increase in the magnetostriction due to the substantial increase of the magnetostrictive phase (ie $BiFeO_3$). For higher concentrations of nanoparticle in the polymer matrix, magnetoelectric coupling coefficient of 2.4 V/cmOe is obtained. Even if BFO thin films show good magnetoelectric coupling at room temperature,[85] they often show high leakage currents due to oxygen vacancies and mixed Fe valences.[86,87] However, multilayer heterostructures of $BiFeO_3$ show high magnetoelectric (ME) coefficients. $BiFeO_3$-$BaTiO_3$ composite film have a ME coefficient up to 2.4 V/cmOe at 300 K which is much higher than that of a single-phase $BiFeO_3$ reference film (4.2 V/cmOe).[86] Fig. 11 shows the ME voltage variations of the film samples with DC magnetic field.

3.3 Magnetic study

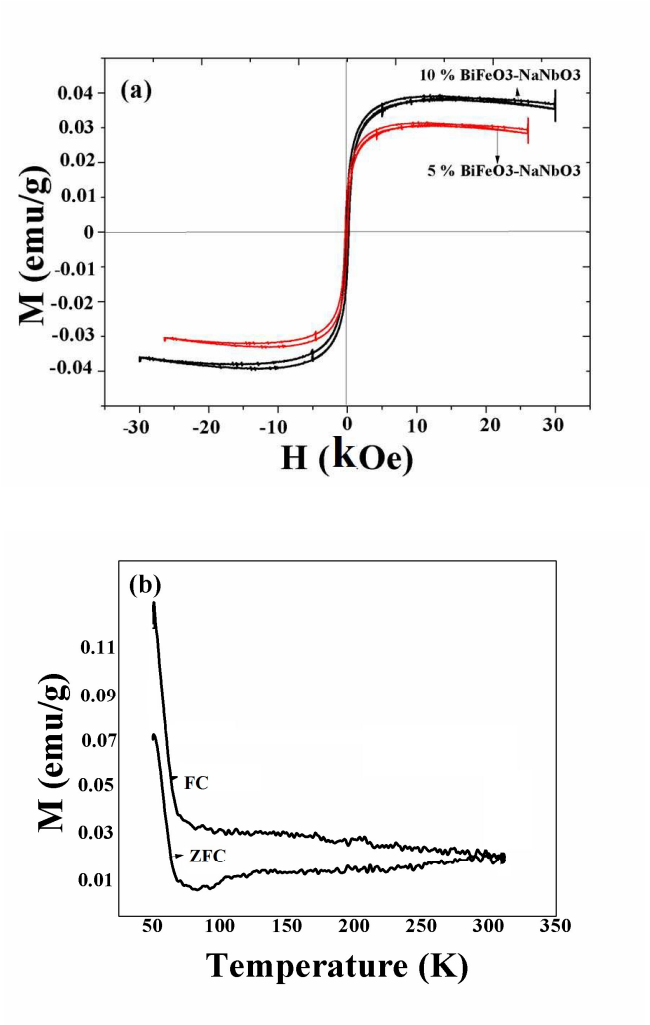

Fig. 12 (a) Hysteresis loop of the 5% $BiFeO_3$-$NaNbO_3$ and 10 % $BiFeO_3$-$NaNbO_3$ in PVDF-TrFE matrix, (b) Temperature dependent magnetization study of 10 % $BiFeO_3$-$NaNbO_3$ in PVDF-TrFE matrix.

Magnetic hystersis loop of 5% $BiFeO_3$ -$NaNbO_3$ and 10 % $BiFeO_3$-$NaNbO_3$ in PVDF-TrFE matrix at room temperature is shown in Figure 12 (a). A good hysteresis behaviour which is saturated within the field of 30 KOe can be observed indicating a ferromagentic nature at room temperature. The ferromagnetism of these samples could be a result of the reduction of particle size. The weak ferromagnetism observed in BFO nanoparticles is due to the nonexact compensation of the spins with a decrease in particle size.[97] When the particle size decreases,

number of surface asymmetry atoms increases. Due to this, the angle of the helical ordered spin arrangement is changed and a net magnetic moment appears.[99,101-105]

The main possibility is the high piezoelectricity due to the presence of P(VDF-TrFE) co-polymer and the other is due to the $NaNbO_3$ content which also has good electromechanical property.[37] Since the XRD patterns have not detected any impurity phase, the properties which have been observed could be due to the contribution of the ceramic part and co-polymer itself. The maximum magnetization attained is different for two compositions and found to be 0.04 emu/g for 10 % $BiFeO_3$ -$NaNbO_3$ and 0.03 emu/g for 5% of $BiFeO_3$-$NaNbO_3$ in P(VDF-TrFE) matrix. The magnetization value is found to be increasing with increase in the amount of nanoparticle in the polymer matrix. While the coercivity (Hc) and remanant magnetization (Mr) are almost same for the two compositions. The coercive field (Hc) is almost 0.9 kOe for both compositions. The ZFC and FC curves of 10 % $BiFeO_3$-$NaNbO_3$ powder in the PVDF-TrFE matrix measured under a magnetic field of 200 Oe is shown in Fig. 12 (b). The divagation of ZFC and FC magnetizations close to room temperature shows the room temperature multiferroic property of the sample and also the spin glass behaviour.[100] These results are consistent with the phenomenon observed in $BiFeO_3$ nanoparticles.[89,90] In the case of non magnetic materials there will not be any difference in the FC and ZFC curve.[17,100] Some reports indicate that the splitting of FC-ZFC curve is due to the coexistance of antiferromagnetic and ferromagnetic phases which is usually observed in core shell type $BiFeO_3$ nanoparticles.[98] The FC and ZFC magnetizations increases gradually with decreasing temperature, and it shows an anomalous behaviour below 100 K which may be due to the superparamagnetic behaviour commonly observed in BFO.[89,90] The study lead by T.J.Park et.al reports a size reduction from bulk to nano change the paramagnetic substance to ferromagnetic.[89]

3.4 Electric study

The frequency dependence of real part of dielectric permittivity (Ɛ) and dielectric loss (tan δ) of $BiFeO_3$-$NaNbO_3$ ceramics at room temperature is plotted in Fig. 13 which follows inverse dependence on frequency, normally followed by almost all ferroelectric materials. Compared to the dielectric properties of $BiFeO_3$, the present composite film samples possess larger ε whereas the dielectric loss is obviously reduced.[91,92]

The dielectric constant of the ceramic polymer composite is very high for the $BiFeO_3$-$NaNbO_3$ volume fraction of 10 vol %, which is the highest dielectric constant reported so far for the polymer composite materials. A nearly good value of dielectric constant for polymer ceramic composite is observed in $BaTiO_3$-PVDF composite.[93,95] The ultra-high dielectric constant can be caused by conductive behavior or electric heterogeneous nature of the composites or interfacial polarization among ceramic-polymer interfaces. In the electrical property of polycrystalline samples, the grain boundary region plays an important role. The inhomogeneity between the grain and grain boundary regions and reduction of movable charges is one of the reasons for ultrahigh value of dielectric constant.[94]

.

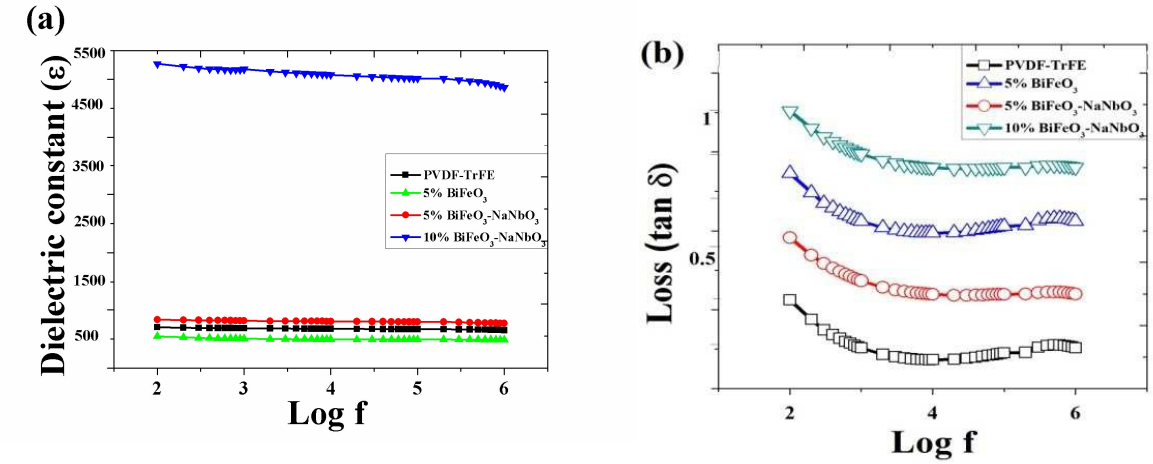

Fig. 13 Dielectric relaxation (a) the real part (b) the imaginary part of dielectric dispersion of $BiFeO_3$ - $NaNbO_3$-P(VDF-TrFE) composite film samples.

The dielectric constant of the ceramic polymer composite is more than 5000 for the $BiFeO_3$–$NaNbO_3$ volume fraction of 10 vol %, which is the highest dielectric constant reported so far for the polymer composite materials. The dielectric constant of the film for $BiFeO_3$ alone in the polymer matrix is less than pure P(VDF-TrFE) as $BiFeO_3$ has a low dielectric compared to P(VDF-TrFE) and $NaNbO_3$. The dielectric constant of the composite increases with increasing vol % of $BiFeO_3$-$NaNbO_3$ ceramics which indicate the dielectric property can be tuned by changing the $NaNbO_3$ content. The decaying trend of dielectric loss with frequency can be ascribed to reduced Ohmic and polarization losses. As a matter of fact, frequency increase is equivalent to reduced available times for free electrons to travel throughout the conductive network in each half cycle of alternating field, i.e. reduced Ohmic loss. Furthermore, due to

interfacial polarization relaxation, the interfacial charge polarization decays with frequency leading to low dipole moment and polarization loss

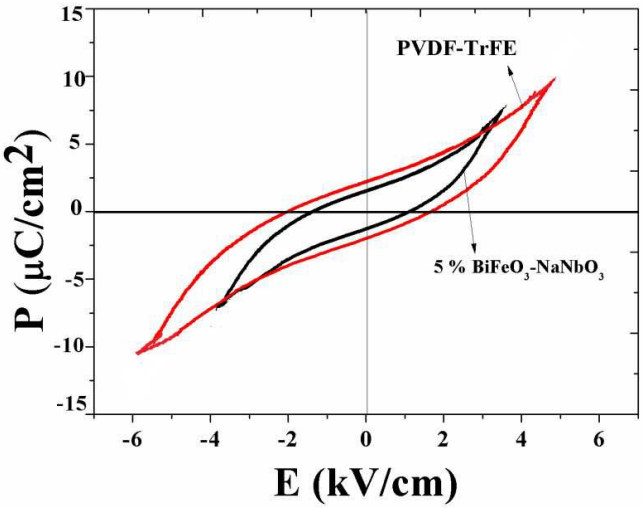

Fig. 14 Ferroelectric hysteresis loop of PVDF-TrFE and 5% $BiFeO_3$-$NaNbO_3$ in P(VDF-TrFE) matrix

Ferroelectric polarization-electric field (PE) loops of 5% $BiFeO_3$-$NaNbO_3$ in P(VDF-TrFE) and pure P(VDF-TrFE) are shown in Fig. 14. The polarization value of pure P(VDF-TrFE) is higher than that of ceramic-polymer composite. It means that the electric polymer P(VDF-TrFE) contribute mainly to the electric property of our samples. Pure co-polymer shows PE loop with a coercive field (Ec) of 2kV/cm and saturation polarization of 10.9 $\mu C/cm^2$ which is consistent with the previous reports of P(VDF-TrFE).[96] The ceramic-polymer composite have saturation polarization of 8 $\mu C/cm^2$ which is mainly due to the ferroelectric phase of co-polymer and $NaNbO_3$. Probably the smaller volume fraction of the polymer phase may be the reason for reduction of polarization value in the ceramic-polymer composite compared to PVDF-TrFE alone. Both the remanant polarization and coercive field are high for P(VDF-TrFE) than the ceramic-polymer composite.

4. Conclusion

Our findings lead to a novel way for preparing energy storing and transforming materials with ultrahigh dielectric constant and room temperature magnetoelectric coupling which are required

in embedded capacitors, microelectromechanical systems, ultrasonic resonators, high power transducers, actuators etc. A series of $BiFeO_3$-$NaNbO_3$-P(VDF-TrFE) composite films with various volume fraction of $BiFeO_3$-$NaNbO_3$ in the polymer matrix were prepared by using spin coating technique. The nanocomposite containing 10 vol % of $BiFeO_3$-$NaNbO_3$ ceramics in the polymer have an ultrahigh dielectric constant at 1 kHz frequency which is very much higher than pure P(VDF-TrFE) and pure BFO. The high d_{33} value observed is a remarkable improvement which alter the magnetic and electric properties of the composite. The room temperature ferromagnetism and magnetoelectric coupling promise tailored applications of current material in various fields. In summary, the giant enhancement in dielectric property as well as magnetoelectric coupling in the film sample make them essential for visualizing the real application of multiferroics. Hence in the design of advanced multiferroic materials, multiphase $BiFeO_3$-$NaNbO_3$-P(VDF-TrFE) composite film is an attractive and successful approach to overcome the limitations of intrinsic single phase multiferroics.

Acknowledgement

The authors would like to acknowledge the financial support from DST – Govt. of India through the Nano Mission, PURSE, FIST Programs, and UGC – Govt. of India for the SAP program. We also express our gratitude to Mr. Sreenivas, APE Research Italy for the PFM measurements. One of the authors RPU would like to acknowledge UGC-Govt. of India for the RFSMS fellowship.

References

1. Wei Qin, Beibei Xu, Shenqiang Ren, Nanoscale, 2015, 7, 9122-9132.
2. Gabriel Caruntu, Amin Yourdkhani, Marian Vopsaroiu, Gopalan Srinivasan, Nanoscale, 2012, 4, 3218-3227.
3. Shujie Sun, Yan Huang, Guopeng Wang, Jianlin Wang, Zhengping Fu, Ranran Peng, Randy J. Knize, Yalin Lu, Nanoscale, 2014, 6, 13494-13500.
4. Hongchen Miao, Xilong Zhou, Shuxiang Dong, Haosu Luo, Faxin Li, Nanoscale, 2014, 6, 8515-8520.

5. Harsh Trivedi, Vladimir V. Shvartsman, Doru C. Lupascu, Marco S. A. Medeiros, Robert C. Pullar, Andrei L. Kholkin, Pavel Zelenovskiy, Andrey Sosnovskikh, Vladimir Ya. Shur, Nanoscale, 2015, 7, 4489-4496.
6. B. Y. Wang, H. T. Wang, Shashi, B. Singh, Y. C. Shao, Y. F. Wang, C. H. Chuang, P. H. Yeh, J. W. Chiou, C. W. Pao, H. M. Tsai, H. J. Lin, J. F. Lee, C. Y. Tsai, W. F. Hsieh, M. H. Tsaif, W. F. Pong, RSC Adv, 2013, 3, 7884.
7. B. Raneesh, A. Saha, D. Das, P. Sreekanth, R. Philip, Nandakumar Kalarikkal, RSC Adv, 2015, 5, 12480.
8. Julie Allibe, Stephane Fusil, Karim Bouzehouane, Christophe Daumont, Daniel Sando, Eric Jacquet, Cyrille Deranlot, Manuel Bibes, Agnes Barthe, Nano Lett. 2012, 12, 1141−1145
9. M. Stingaciu, P. G. Reuvekamp, C. W. Tai, R. K. Kremer, M. Johnson, J. Mater. Chem. C, 2014, 2, 325.
10. C. Binek, Physics, 2013, 6, 13.
11. G. Lawes, G. Srinivasan, J. Phys. D Appl. Phys, 2011, 44, 243001.
12. V. V. Lazenka, G. Zhang, J. Vanacken, I. Makoed, A. F. Ravinski, V. V. Moshchalkov, J. Phys. D Appl. Phys,2012, 45, 125002.
13. J. Ma, J. Hu, Z. Li, C. W. Nan, Adv. Mater., 2011, 23, 1062.
14. C. A. F. Vaz, J. Hoffman, C. H. Ahn, R. Ramesh, Adv. Mater., 2010, 22, 2900.
15. P. Martins, S. Lanceros M endez, Adv. Funct. Mater., 2013, 23, 3371.
16. N. Lei, S. Park, P. Lecoeur, D. Ravelosona, C. Chappert, Phys. Rev. B, 2011, 84, 012404.
17. O. D. Jayakumar, B. P. Mandal, J. Majeed, G. Lawes, R. Naik, A. K. Tyagi, J. Mater. Chem. C, 2013, 1, 3710.
18. M. Li, Y. Wang, Y. Shen, J. Gao, J. Li, D. Viehland, J. Appl. Phys., 2013, 114, 144501.
19. Y. Chen, J. Wang, M. Liu, J. Lou, N. X. Sun, C. Vittoria, V. G. Harris, Appl. Phys. Lett., 2008, 93, 112502.
20. Z. Zhou, T. X. Nan, Y. Gao, X. Yang, S. Beguhn, M. Li, Y. Lu, J. L. Wang, M. Liu, K. Mahalingam, B. M. Howe, G. J. Brown, N. X. Sun, Appl. Phys. Lett., 2013, 103, 232906.
21. R. Jahns, A. Piorra, E. Lage, C. Kirchhof, D. Meyners, J. L. Gugat, M. Krantz, M. Gerken, R. Knochel, E. Quandt, J. Am. Ceram. Soc., 2013, 96, 1673–1681.

22. H. Zhao, X. Peng, L. Zhang, J. Chen, W. Yan, X. Xing, Appl. Phys. Lett, 2013, 103, 082904.
23. N. Jedrecy, H. J. von Bardeleben, V. Badjeck, D. Demaille, D. Stanescu, H. Magnan, A. Barbier, Phys. Rev. B, 2013, 88, 121409.
24. W. Liang, Z. Li, Z. Bi, T. Nan, H. Du, C. Nan, C. Chen, Q. Jia Y. Lin, J. Mater. Chem. C, 2014, 2, 708–714.
25. S. Mukherjee, A. Roy, S. Auluck, R. Prasad, R. Gupta, A. Garg, Phys. Rev. Lett., 2013, 111, 087601.
26. Zhai, Z. Xing, S. Dong, J. Li, D. Viehland, J. Am. Ceram. Soc., 2008, 91, 351–358.
27. Y. Lin, N. Cai, J. Zhai, G. Liu, C. W. Nan, Phys. Rev. B, 2005, 72, 012405.
28. N. Lei, S. Park, P. Lecoeur, D. Ravelosona, C. Chappert, Phys. Rev. B, 2011, 84, 012404.
29. M. Liu, O. Obi, Z. Cai, J. Lou, G. Yang, K. S. Ziemer, N. X. Sun, J. Appl. Phys., 2010, 107, 073916.
30. J. Lou, M. Liu, D. Reed, Y. Ren, N. X. Sun, Adv. Mater., 2009, 21, 4711.
31. Z. Wang, R. Viswan, B. Hu, J. F. Li, V. G. Harris, D. Viehland, J. Appl. Phys., 2012, 111, 034108.
32. Z. Li, J. Hu, L. Shu, Y. Gao, Y. Shen, Y. Lin, C. W. Nan, J. Appl. Phys., 2012, 111, 033918.
33. C. Pettiford, J. Lou, L. Russell, N. X. Sun, Appl. Phys. Lett., 2008, 92, 122506.
34. F. Zighem, D. Faurie, S. Mercone, M. Belmeguenai, H. Haddadi, J. Appl. Phys., 2013, 114, 073902.
35. M. Weiler, A. Brandlmaier, S. Gepreags, M. Althammer, M. Opel, C. Bihler, H. Huebl, M. S. Brandt, R. Gross, S. T. B. Goennenwein, New J. Phys., 2009, 11, 013021.
36. Brandlmaier, S. Gepreags, G. Woltersdorf, R. Gross, S. T. B. Goennenwein, J. Appl. Phys., 2011, 110, 043913.
37. C. W. Nan, Phys. Rev. B, 50, 1994, 6082–6088.
38. C. H. Sim, A. Pan and Wang, J. Appl. Phys., 2008, 103, 124109.
39. Dipanjan Mazumdar, Vilas Shelke, Milko Iliev, Stephen Jesse, Amit Kumar, Sergei V. Kalinin, Arthur P. Baddorf, Arunava Gupta, Nano Lett. 2010, 10, 2555–2561.
40. Rehana. P. Ummer, P. Sreekanth, B. Raneesh, Reji Philip, Didier Rouxel, Sabu Thomas, Nandakumar Kalarikkal, RSC Adv., 2015, 5, 67157.

41. Mitoseriu L et al,J. Eur. Ceram. Soc. 2007, 27, 4379–82.
42. Shaobo Tan, Xin Hu, Shujiang Ding, Zhicheng Zhang, Huayi Li, Lanjun Yang, J. Mater. Chem. A, 2013, 1, 10353.
43. Y. Feng, W. L. Li, Y. F. Hou, Y. Yu, W. P. Cao, T. D. Zhanga W. D. Fei, J. Mater. Chem. C, 2015, 3,1250.
44. Cross, L. E. Jpn. J. Appl. Phys.,1995, 5, 34.
45. M. V. Gandhi, Thomson, B. S., Chapman and Hall Publishing group, L London 1992, Vol 5, 310, pp.,
46. Y. C. Zhou, Y. Y. Bai, K. Yu, Y. Kang H. Wang, Appl. Phys. Lett, 2013, 102, 252903–252905.
47. T. Zhou, J. W. Zha, R. Y. Cui, B. H. Fan, J. K. Yuan, Z. M. Dang, ACS Appl. Mater. Interfaces, 2011, 3, 2184–2188.
48. W. M. Xia, Z. Xu, F. Wen, Z. C. Zhang, Ceram. Int., 2012, 38, 1071–1075.
49. V.S. Nguyen, L. Badie, E. Senechault, E. Blampain, B. Vincent, C. Venet, et al Ieee Trans. Ultrason. Ferroelectr. Freq. Control., 2013, 60, 2039–2043.
50. S. G. Lu, J. Z. Jin, X. Zhou, Z. Fang, Q. Wang, Journal of Applied Physics, 2011, 110, 10-11.
51. Xiaohua Liu, Shuangyi Liu, MyungGeun Han, Lukas Zhao, Haiming Deng, Jackie Li, Yimei Zhu, Nanoscale Research Letters, 2013, 8, 37.
52. N. Jedrecy, H. J. von Bardeleben, V. Badjeck, D. Demaille, D. Stanescu, H. Magnan, A. Barbier, Phys. Rev. B, 2013, 88, 121409.
53. W. Liang, Z. Li, Z. Bi, T. Nan, H. Du, C. Nan, C. Chen, Q. Jia, Y. Lin, J. Mater. Chem. C, 2014, 2, 708–714.
54. S. Mukherjee, A. Roy, S. Auluck, R. Prasad, R. Gupta, A. Garg, Phys. Rev. Lett., 2013, 111, 087601.
55. Zhai, Z. Xing, S. Dong, J. Li, D. Viehland, J. Am. Ceram. Soc., 2008, 91, 351–358.
56. Y. Lin, N. Cai, J. Zhai, G. Liu, C. W. Nan, Phys. Rev. B, 2005, 72, 012405
57. B. Chu, X. Zhou, K. Ren, B. Neese, M. Lin, Q. Wang, F. Bauer, Q. M. Zhang, Science, 2006, 313, 334.
58. Z. M. Dang, Y. H. lin, C. W. Nan, Adv. Mater., 2003, 15, 1625.
59. Q. Gao, J. I. Scheinbeim, B. A. Newman, J. Polym. Sci. B, 1999, 37

60. V. S. Nguyen, L. Badie, E. Senechault, E. Blampain, B. Vincent, C. Venet, et al Ieee Trans. Ultrason. Ferroelectr. Freq. Control., 2013, 60, 2039–2043
61. V. S. Nguyen, L. Badie, E. Lamouroux, B. Vincent, F.D. Dos Santos, M. Aufray, et al., J. Appl. Polym. Sci., 2013, 129, 391–396.
62. V. S. Nguyen, D. Rouxel, B. Vincent, L. Badie, F. D. Dos Santos, E. Lamouroux, et al., Appl. Surf. Sci., 2013, 279, 204–211.
63. V. S. Nguyen, D. Rouxel, M. Meier, B. Vincent, A. Dahoun, S. Thomas, et al., Polym. Eng. Sci., 2014, 54, 1280–1288.
64. W. M. Xia, Z. Xu, F. Wen, Z. C. Zhang, Ceram. Int., 2012, 38, 1071–1075.
65. Q. M. Zhang, H. Li, M. Poh, F. Xia, Z. Y. Cheng, H. Xu, C. Huang, Nature (London), 2002, 419, 284.
66. S. X. Huo, S. L. Yuan, Y. Qiu, Z. Z. Ma, C. H. Wang, J. Material letters, 2012, 68, 8-10.
67. J. Xu, H. Ke, D. Jia, J. Alloy. Compd., 2009, 472, 473——7
68. K. Tashiro, M. Kobayashi, Spectrochim. Acta 50A, 1994, 1573.
69. K. J. Kim, N. M. Reynolds, S. L. Hsu, Macromolecules, 1989, 22, 4395.
70. N. M. Reynolds, K. J. Kim, C. Chang, S. L. Hsu, Macromolecules, 1989, 22, 1092.
71. K. J. Kim, N. M. Reynolds, S. L. Hsu, J. Polym. Sci., Part B Polym. Phys. 31, 1993, 1555.
72. M. H. Nguyen, S. Lee, W. M. Kriven, J. Mater.Res, 1999, 14, 3417-26.
73. S. Ghosh, S. Dasgupta, A. Sen, H. S. Maiti, J. Am. Ceram. Soc., 2005, 88, 1349-52.
74. H. Zhang, X. Fu, S. Niu, Q. Xin, J. Alloys Compd., 2008, 457, 61–65.
75. S. K. Pradhan, J. Mater Sci. Mater Electron, 2013, 24, 3581–3586.
76. E. Heracleous, A. A. Lemonidou, J. Catal., 2006, 237, 162–174.
77. J. M. Jehng, I. E. Wachs, Chem. Mater., 1991, 3, 100–107.
78. B. X. Huang, K. Wang, J. S. Church, Y. S. Li, Electrochim. Acta,1999, 44, 1999, 2571–2577.
79. P. F. Graca, M.G.Ferreirada Silva, M. A. Valente, Solid StateSci., 2009, 11, 570–577.
80. Coondoo. I, Panwar. N, Bdikin. I, Puli. V.S, Katiyar. R.S, Kholkin AL, J Phys D: Appl Phys., 2012, 45, 055302.
81. Kholkin A, Bdikin I, Ostapchuk T, Petzelt, J. Appl Phys Lett., 2008, 93, 222905.
82. M. Berlincourt, D. Krueger. H, J. Appl. Phys, 30, 1804-1810.

83. Damjanovic. D, Demartin M, J. Phys. Condens. Matter, 1997, 9, 4943,
84. Xiaohua Liu, Shuangyi Liu, MyungGeun Han, Lukas Zhao, Haiming Deng, Jackie Li, Yimei Zhu, Nanoscale Research Letters, 2013, 8, 37
85. P. Rovillain, R. de Susa, Y. Gallais, A. Sacuto, M. A. Measson, D. Colson, A. Forget, M. Bibes, A. Barth_el_emy, M. Cazayous, Nat. Mater, 2010, 9, 975.
86. G. W. Pabst, L. W. Martin, Y. H. Chu R. Ramesh, J. Appl. Phys. Lett. 2007,90, 072902.
87. F. Bern, P. Schwinkendorf, A. Setzer, M. Lorenz, M. Grundmann, I. Vrejoiu and M. Ziese, 2014,J. Phys. Condens. Matter, 47, 135303.
88. Michael Lorenz, Gerald Wagner, Vera Lazenka, Peter Schwinkendorf, HiwaModarresi, Margriet J. Van Bael, Andre Vantomme, KristiaanTemst, Oliver Oeckler, Marius Grundmann, J.App.Phys. letters,2015, 106, 012905.
89. T. J. Park, G. C. Papaefthymiou, A. J. Viescas, A. R. Moodenbaugh S. S. Wong, Nano Lett., 2007, 7, 766–772 .
90. B. Liu, B. Hu and Z. Du, Chem. Commun., 2011, 47, 8166–8168.
91. M. M. Kumar, V. R. Palkar, K. Srinivas, S. V. Suryanarayana, Appl. Phys. Lett., 2000, 76, 2764.
92. A. K. Pradhan, K. Zhang, D. Hunter, J. B. Dadson, G. B. Loutts, P. Bhattacharya, R. Katiyar, J. Zhang, D. J. Sellmyer, U. N. Roy, Y. Cui, A. Burger, J. Appl. Phys, 2005, 97,93-90.
93. Z. M. Dang, L. Z. Fan, Y. Shen, C. W. Nan, J. Materials Science and Engineering B, 2003,103, 140-144.
94. S. Manna, T. Ghoshal, S. K. De, J. Phys. D Appl. Phys., 2010,43, 295403
95. Tushar Sharma, Sang-Soo Je, Brijesh Gill, John X.J. Zhang, Sensors and Actuators A,12012, 77, 87– 92.
96. Matthias Dietze, Mohammed Es-Souni, Sensors and Actuators A, 2008, 143, 329–334
97. J. C. Denardin, A. L. Brandl, M. Knobel, P. Panissod, A. B. Pakhomov, H. Liu, X. X. Zhang, Phys. Rev. B: Condens. Matter, 2002, 65, 064422
98. Huang, F. Z. et al., Thin Solid Films, 2012, 520, 6489–6492.
99. B. Kumari, P. R. Mandal, T. K. Nath, Adv. Mat. Lett., 2014, 5(2), 84-88.

100. Manoj K. Singh, W. Prellier, M. P. Singh, Ram S. Katiyar, J. F. Scott, Phys. Rev.B, 2008, **77**, 144403
101. Mazumder R, SujathaDevi P, Bhattacharya D, Choudhury P, Sen A, Raja M, Appl. Phys. Lett, 2007, 91, 062510.
102. R.V.K. Mangalama, Nirat Ray b , Umesh V. Waghmare b, A. Sundaresana, C.N.R. Rao, Solid State Communications, 2009, 149, 1–5.
103. T. J. Park, G. C. Papaefthymiou, A. J. Viescas, A. R. Moodenbaugh, S. S. Wong, Nano Lett., 2007, 7, 766–772 .
104. B. Liu, B. Hu, Z. Du, Chem. Commun., 2011, 47, 8166–8168.
105. J. C. Denardin, A. L. Brandl, M. Knobel, P. Panissod, A. B. Pakhomov, H. Liu, X. X. Zhang, Phys. Rev. B: Condens. Matter, 2002, 65, 064422.

Figure captions

Fig. 1: The typical configuration of the prepared thin film sample

Fig. 2: (a) Crystal structure of PVDF different phases. (b) X-ray diffractogram of composite film samples for various nanoparticle concentrations in the polymer matrix.

Fig. 3: SEM of $BiFeO_3$-$NaNbO_3$–P(VDF–TrFE) composite film samples for, (a) P(VDF-TrFE) alone, (b) 5% $BiFeO_3$ in the P(VDF-TrFE) matrix, (c) 5% $BiFeO_3$-$NaNbO_3$ in the P(VDF-TrFE) matrix, (d) 10% $BiFeO_3$-$NaNbO_3$ in the P(VDF-TrFE) matrix.

Fig. 4: TEM images of $BiFeO_3$-$NaNbO_3$- P(VDF-TrFE) composite film samples for (a) 5 % $BiFeO_3$ in the polymer matrix (b) 5% $BiFeO_3$-$NaNbO_3$ in the polymer matrix (c) HRTEM image of 5 % $BiFeO_3$ - $NaNbO_3$ in the polymer matrix.

Fig. 5 (a) 2D AFM image of 5% $BiFeO_3$-$NaNbO_3$ in the polymer matrix, (b) 3D AFM image of 5% $BiFeO_3$-$NaNbO_3$ in the polymer matrix, (c) 2D AFM image of 10% $BiFeO_3$-$NaNbO_3$ in the polymer matrix, (d) 3D AFM image of 10% $BiFeO_3$-$NaNbO_3$ in the polymer matrix

Fig. 6 The phase images of the samples (a) 5% $BiFeO_3$-$NaNbO_3$ in polymer matrix, (b) 10% $BiFeO_3$-$NaNbO_3$ in polymer matrix.

Fig. 7: FTIR spectra of $BiFeO_3$-$NaNbO_3$-PVDF TrFE composite film samples for (a) P(VDF-TrFE) alone, (b) 5% $BiFeO_3$ in the P(VDF-TrFE) matrix, (c) 5% $BiFeO_3$-$NaNbO_3$ in the P(VDF-TrFE) matrix, (d) 10% $BiFeO_3$-$NaNbO_3$ in the P(VDF-TrFE) matrix.

Fig. 8: Confocal raman spectra of $BiFeO_3$-$NaNbO_3$-P(VDF-TrFE) composite film samples for (a) P(VDF-TrFE) alone, (b) 5 % $BiFeO_3$ in the P(VDF-TrFE) matrix, (c) 5 % $BiFeO_3$-$NaNbO_3$ in the P(VDF-TrFE) matrix, (d) 10% $BiFeO_3$-$NaNbO_3$ in the P(VDF-TrFE) matrix.

Fig. 9 : (a) Surface topography of 5% $BiFeO_3$- $NaNbO_3$ in the polymer matrix (b) Surface topography of 10% $BiFeO_3$- $NaNbO_3$ in the polymer matrix (c) PFM image of 5% $BiFeO_3$-$NaNbO_3$ in the polymer matrix (d) PFM image of 10 % $BiFeO_3$- $NaNbO_3$ in the polymer matrix.

Fig. 10: ME voltage as a function of AC magnetic field at different fixed DC field for $BiFeO_3$-$NaNbO_3$ – P(VDF-TrFE) composite film samples for (a) P(VDF-TrFE) alone, (b) 5% $BiFeO_3$ in the P(VDF-TrFE) matrix, (c) 5% $BiFeO_3$-$NaNbO_3$ in the P(VDF-TrFE) matrix, (d) 10% $BiFeO_3$-$NaNbO_3$ in the P(VDF-TrFE) matrix.

Fig. 11: ME voltage as a function of DC magnetic field for $BiFeO_3$-$NaNbO_3$-P(VDF-TrFE) composite film samples for (a) P(VDF-TrFE) alone, (b) 5 % $BiFeO_3$ in the P(VDF-TrFE) matrix, (c) 5% $BiFeO_3$-$NaNbO_3$ in the P(VDF-TrFE) matrix, (d) 10% $BiFeO_3$-$NaNbO_3$ in the P(VDF-TrFE) matrix.

Fig. 12 : (a) Hysteresis loop of the 5% $BiFeO_3$-$NaNbO_3$ and 10 % $BiFeO_3$-$NaNbO_3$ in PVDF-TrFE matrix, (b) Temperature dependent magnetization study of 10 % $BiFeO_3$-$NaNbO_3$ in PVDF-TrFE matrix.

Fig. 13: Dielectric relaxation (a) the real part, (b) the imaginary part of dielectric dispersion of $BiFeO_3$ - $NaNbO_3$-P(VDF-TrFE) composite film samples.

Fig. 14: Ferroelectric hysteresis loop of PVDF-TrFE and 5% $BiFeO_3$-$NaNbO_3$ in P(VDF-TrFE) matrix

Table captions

Table 1 : Details of the film samples

Table 2: The d_{33} values determined by Berlincourt method

Table 3 : Calculated values of magnetoelectric coupling coefficient (α)